JOURNAL OF INFORMATION SCIENCE AND ENGINEERING 39, 825-838 (2023)
DOI: 10.6688/JISE.202307_39(4).0008

A Novel Joint Frequency Offset Estimation Scheme for OFDM System

QIAN DU[1], ZHAO-FENG WU[4], JUN WANG[2,+], WEN-WU XIE[4,+] AND YA-LAN LI[2,3,+]
[1]*Department of Information Science and Engineering*
Linyi University
Linyi, Shandong Province, 276000 P.R. China
E-mail: duqian@lyu.edu.cn
[2]*School of Electronic Information and Electrical Engineering*
[3]*Hunan Engineering Research Center of Advanced Embedded Computing and Intelligent Medical Systems*
Xiangnan University
Chenzhou, Hunan Province, 423000 P.R. China
E-mail: junwang_cn@qq.com; liyalan@xnu.edu.cn
[4]*Department of Information and Communication Engineering*
Hunan Institute of Science and Technology
Xiangtan, Hunan Province, 411100 P.R. China
E-mail: gavinxie@hnist.edu.cn; wuzhaofenga@163.com

With the fast development of wireless mobile communication networks, the 4th and 5th-generation wireless mobile communication systems are now applied in different fields. They can be efficiently used in land–air wireless communication to provide wireless Internet services for passengers on civilian aircrafts. The frequency offset estimation (FOE) is an important issue in land–air wireless communication environment. Accordingly, a novel joint FOE scheme based on the orthogonal frequency division multiplexing system is proposed in this paper. Firstly, this paper proposes a new FOE algorithm based on the peak power ratio (PPR) on the physical random-access channel (PRACH). Secondly, a joint FOE scheme is proposed, which uses the conventional FOE based on the physical uplink shared channel and the proposed PPR FOE based on PRACH. The proposed joint FOE scheme can extend the range of FOE from [−1000 Hz, 1000 Hz] to [−1875 Hz, 1875 Hz] and has better performance than the proposed PPR FOE method and the conventional FOE.

Keywords: frequency offset estimation, peak power ratio, OFDM, 4G, 5G

1. INTRODUCTION

With the fast development of wireless communication technology, the fourth generation (4G) and the fifth generation (5G) wireless communication technology have been used in many industries to achieve wireless communication. For instance, land-air wireless communication aims to provide wireless Internet services to passengers on civilian aircrafts. Aircrafts usually fly at a speed ranging from 800 km/h to 1000 km/h, so the impact of the Doppler frequency shift for land-air wireless communication is very serious. The study on

Received June 12, 2022; revised July 6 & August 11, 2022; accepted September 13, 2022.
Communicated by Mu-Yen Chen.
[+] Corresponding authors: junwang_cn@qq.com; gavinxie@hnist.edu.cn; liyalan@xnu.edu.cn.
[*] This work was supported by the Open Fund of Advanced Cryptography and System Security Key Laboratory of Sichuan Province under Grant SKLACSS-202115, the Natural Science Foundation of Hunan Province under Grant 2020JJ4341, the Key Projects of Hunan Provincial Department of Education Department under Grant 21A0408, the Applied Characteristic Disciplines of Electronic Science and Technology of Xiangnan University (XNXY20221210), "The 14th Five-Year Plan" of Educational and Scientific Research (Lifelong Education Research Base Fundamental Theory Area) in Hunan Province(XJK22ZDJD58).

the Doppler frequency shift for wireless communication is an old topic, but such a speed is generally limited to less than 350 km/h. This study focuses on the impact of the Doppler frequency shift on wireless communication at speeds ranging from 800 to 1000 km/h.

The main challenge in the land-air wireless communication system based on 4G and 5G technology is the influence of the Doppler frequency shift in ultra-high-speed environments. This problem is usually solved by adopting the orthogonal frequency division multiplexing (OFDM) technology. Moreover, it is necessary to estimate and compensate the frequency offset of the OFDM system to reduce the interference. Aiming at the frequency synchronisation of OFDM-based wireless communication systems, many scholars have performed considerable research works and put forward many frequency offset estimation (FOE) algorithms for the OFDM system, which can be divided into three categories: FOE algorithm based on the cyclic prefix [1-14] and non-data-assisted blind FOE algorithm [15-22] and data-assisted FOE algorithm [23-42]. Specifically, some papers [1, 2] used the Maximum-likelihood estimation to calculate frequency offset approximately. Papers [8, 10] took into accounts the symbol synchronization or frame synchronization of the system. Besides, papers [15-22] used the non-data-assisted blind FOE algorithms. Among them, the paper [22] proposed an efficient carrier estimator, which is very instructive for this paper.

With the fast development of 4G and 5G wireless communication technology, more papers [30-41] have studied the FOE based on a 4G system than before. A joint estimation of the carrier and sampling frequency offset for LTE Advanced UL multiple-input and multiple-output was proposed in [30]. The papers [31] and [32] proposed a scheme to estimate the time and frequency offsets based on the LTE downlink system. Based on the method in [23], paper [39] studied the time and frequency offsets for the LTE UL system.

In this paper, a novel joint FOE scheme based on the OFDM system is proposed. Firstly, a new FOE algorithm of the peak power ratio (PPR) is proposed based on the physical random-access channel (PRACH). Secondly, we propose a joint FOE scheme, which used the conventional FOE [23, 39] based on PUSCH and the PPR FOE based on PRACH. Simulation results show that the proposed joint FOE can get better performance and can extend the conventional estimation range of the frequency offset from [−1000 HZ, 1000 Hz] to [−1875 Hz, 1875 Hz].

This paper consists of seven sections: Section 2 describes the system model for land-air wireless communication. Section 3 mainly introduces the conventional FOE algorithm based on the PUSCH of the LTE system. Section 4 presents the proposed PPR FOE based on PRACH, and the proposed PPR FOE algorithm can effectively expand the range of FOE. Section 5 describes the joint FOE algorithm in detail. Section 6 presents the performance analysis and simulation results. Finally, Section 7 gives the conclusions and future work.

2. SYSTEM MODEL

Land–air wireless communication is used for communication on civilian aircrafts, mainly LTE base stations (BSs) along the route from the ground to air coverage. Passengers communicate via Wi-Fi using a custom terminal receiver on civilian aircrafts. In high-speed civilian aircrafts in flight, the aircraft movement rate is usually 800 to 1000 km/h. The impact of the Doppler frequency shift on the aircraft communication causes easier network, cell selection failures and other problems. Therefore, civil aviation communication has put forward high standard requirements for wireless communication systems. The aircraft movement rate is usually 800 to 1000 km/h, so the high-speed LTE system performance covering the scene for the greatest impact effect is the Doppler frequency shift. The LTE route private network requires an excellent frequency tracking and adaptive compensation algorithm to eliminate the enormous high-speed-flight Doppler frequency shift.

The channel model of land–air wireless communication is similar to that of a high-speed train model proposed by [43], which is shown in Fig. 1.

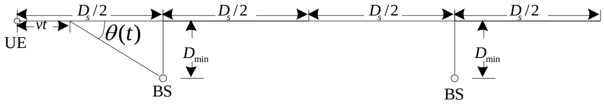

Fig. 1. Motion model of UE versus base station in land–air wireless communication.

In Fig. 1, $D_{\min}$ is the minimum distance between UE and BS, D_S is the coverage radius of BS and v is the velocity of UE. For land-air wireless communication, D_S is usually 100-200 km, $D_{min} > 8$ km and v are usually 800 to 1000 km/h. In the land-air wireless communication channel mode, the Doppler frequency shift is given by

$$f_s(t) = f_d \cos\theta(t) \tag{1}$$

where f_d denotes the maximum value of the Doppler frequency shift, $f_s(t)$ denotes the estimated Doppler frequency shift and $\theta(t)$ represents the angle between the motion direction of UE and the direction from UE to BS.

The maximum value of the Doppler frequency shift f_d is given by

$$f_d = f * v/C \tag{2}$$

where f is the frequency of the signal and C is the propagation velocity of the electromagnetic wave. According to Eq. (2), when v is 1000 km/h and f is 1 GHz, the maximum Doppler frequency shift f_d is 925 Hz, and the maximum Doppler frequency shift of UE is 925 Hz. Because the UE is based on the frequency of the received downlink signal to transmit the UL signal, the BS will withstand the Doppler frequency shift in the terminal twice, and then the maximum Doppler frequency shift of the BS becomes 1850 Hz.

3. CONVENTIONAL FOE SCHEME

PUSCH is mainly used to transmit the data information of the terminal in the LTE system. There are two pilot sequences, *i.e.* two demodulation reference signals, on PUSCH. The two DMRs are in the same transmission time interval (TTI). The reference signal DMRs of PUSCH are mainly used for channel estimation and time and frequency synchronisation.

The base sequence of the DMR signal is a Zadoff-Chu (*ZC*) sequence. A *ZC* sequence is a zero autocorrelation and cross-correlation sequence with a constant amplitude. In addition, the code word of the *ZC* sequence has a wide selection range. According to the system requirements, DMRs can produce different lengths.

In the LTE UL, there are two DMR symbols in one TTI, and the interval between the two DMR symbols is $N_dT_s = 0.5$ ms, where N_d is the sampling interval between the two DMRs. T_s is the sampling period of the PUSCH symbol, and $T_s = 1/(15000\times2048)$.

In the frequency domain, the bandwidth of DMRs is the same as that of a PUSCH data distribution. The two DMR signals in the frequency domain can be expressed as [43]

$$X_i = [x_i(0), \ldots, x_i(L-1)],\ i = 1, 2, \tag{3}$$

where L is the length of the DMR symbol, i is the ith DMR symbol and there are two DMR symbols in one TTI.

In the LTE UL system, the time continuous signal $s_i(t)$ of PUSCH DMRs in an UL TTI can be expressed as [43]

$$s_i(t) = \sum_{n=0}^{L-1} x_i(n)\cdot e^{j2\pi n t f_s}, 0 \le t < (N_{\mathrm{CP}} + N)\times T_{\mathrm{s}}. \tag{4}$$

f_s is the subcarrier interval of the PUSCH symbol, and $f_s = 15$kHz. N_{CP} is the length of CP, and $N = 2048$ [43]. Assuming that the transmission signal $s_i(t)$ passes through a multipath propagation channel with AWGN, the received signal can be expressed as

$$r_i(t) = s_i(t)\otimes h_i(t) + w_i(t), \tag{5}$$

where $h_i(t)$ is the channel impulse response and $w_i(t)$ represents the AWGN with a mean value of 0 and variance of σ_n^2.

Based on the ML estimation algorithm, we can calculate the cross-correlation of the corresponding channel estimation coefficients on the same subcarrier of the two pilot signals, and the formula is expressed as [39]

$$R_f = \sum_{k=0}^{L-1} H_1'(k)^* H_2'(k) \approx e^{j2\pi N_d T_s \Delta f} \sum_{k=0}^{L-1} H_1(k)^* H_2(k) \tag{6}$$

where $H_i(k)$ represents the channel coefficient in the frequency domain. Then, the estimated frequency offset $\Delta f'$ can be obtained by calculating the radiation angle R_f, which is expressed as

$$\Delta f' = \frac{\arg(R_f)}{2\pi N_d T_s}, \tag{7}$$

where N_dT_s is the time interval between two DMR symbols, and $N_dT_s = 0.5$ms. $\arg(R_f)$ is the radial angle of complex number, so we can get

$$\arg(R_f)\in(-\pi, \pi). \tag{8}$$

Based on Eq. (16), we can calculate the range of the estimated frequency offset as

$$\Delta f\in(-1000Hz, 1000Hz). \tag{9}$$

4. PROPOSED PPR FOE SCHEME

In the LTE UL, PRACH is used to transmit the random access channel (RACH) preamble, which is generated from *ZC* sequences with a zero correlation zone, generated from one or several root *ZC* sequences. The *u*th root *ZC* sequence is defined by [43]

$$x_u(n) = e^{-j\frac{\pi un(n+1)}{N_{ZC}}}, \quad 0 \le n \le N_{ZC} - 1, \tag{10}$$

where the length of the *ZC* sequence is denoted by N_{ZC}, which is equal to 839 [43]. For the *u*th root *ZC* sequence, the preamble of length N_{CS} is defined by cyclic shifts according to

$$x_{u,v}(n) = x_u((n+C_v) \bmod N_{ZC}). \tag{11}$$

If Δf denotes the real frequency offset in Hz, then the original sequence of the RACH preamble is $r(n) = x_u(n)$. In addition. With the received $\hat{r}(n)$, the RACH preamble with the frequency offset is

$$\begin{aligned} \hat{r}(n) &= r(n)e^{-j\Delta\omega n} + \psi_1(n) \\ &= x_u(n)e^{-j\Delta\omega n} + \psi_1(n) \end{aligned}, \tag{12}$$

where $\Delta\omega$ denotes the phase to frequency offset Δf and $\Delta\omega = 2\pi\Delta f/f_s$. Then, the AWGN is $\psi_1(n)$, which has a zero mean and variance σ_n^2. If the sampling period of the PRACH symbol is denoted by T_{sym}, then the sampling rate of the RACH preamble f_s can be written as $f_s = 1/T_{sym}$. Then, Eq. (12) can be expressed as

$$\begin{aligned} \hat{r}(n) &= x_u(n)e^{-j2\pi\Delta f\cdot T_{sym}n} + \psi_1(n) \\ &= x_u(n)e^{-j2\pi\Delta f\cdot T_{SEQ}n/N_{ZC}} + \psi_1(n) \end{aligned}, \tag{13}$$

where the length of the preamble sequence is T_{SEQ}. Accordingly, $N_{ZC} = T_{SEQ}/T_{sym}$. If we calculate the cross-correlation between the cyclic shift of the original *ZC* sequence and the receiver preamble sequence, we can derive the power delay profile (PDP) $P(l)$, which can be expressed by

$$P(l) = \left| \sum_{n=0}^{N_{ZC}-1} \hat{r}(n) x_u^*\left((n+l) \bmod N_{ZC}\right) \right|^2, \tag{14}$$

where $l = 0, 1, 2, \ldots, N_{ZC} - 1$. When the frequency offset Δf is $1/T_{SEQ}$, by combining Eqs. (10) and (13), we can derive

$$\begin{aligned} \hat{r}(n) &= e^{-j\frac{\pi un(n+1)}{N_{ZC}}} e^{-j2\pi n/N_{ZC}} + \psi_1(n) \\ &= x_u(n+1/u)\, e^{j\pi(1/u+1)/N_{ZC}} + \psi_1(n). \end{aligned} \tag{15}$$

The cyclic shift period of the preamble sequence is $d_u = (1/u) \bmod N_{ZC}$, and it must be an integer. Thus, $d_u = ((mN_{ZC}+1)/u) \bmod N_{ZC}$, where m is the smallest positive integer. From Eq. (14), when the frequency offset is $1/T_{SEQ}$, the peak power of the cross-correlation between $\hat{r}(n)$ and $r(n)$ will occur at d_u. With Eqs. (14) and (15), the peak power of $P(l)$ at $l = 0$ is given by

$$\begin{aligned} P_{l=0}(\Delta f) &= \left| \sum_{n=0}^{N_{ZC}-1} \hat{r}(n) x_u^*(n) \right|^2 \\ &= \left| \sum_{n=0}^{N_{ZC}-1} \left(\exp\left(-j \frac{2\pi n \Delta f T_{SEQ}}{N_{ZC}} \right) + x_u^*(n) \psi_1(n) \right) \right|^2 . \end{aligned} \tag{16}$$

Because $d_u = ((mN_{ZC}+1)/u) \bmod N_{ZC}$, if the impact of noise $\psi_1(n)$ can be ignored, when $l = \pm kd_u$, the peak power of $P(l)$ is given by

$$\begin{aligned} P_{l=\pm kd_u}(\Delta f) &= \left| \sum_{n=0}^{N_{zc}-1} x_u^*\left((n \pm kd_u) \bmod N_{ZC} \right) \hat{r}(n) \right|^2 \\ &= \left| \frac{\sin\left(\pi(\Delta f T_{SEQ} \pm k) \right)}{\sin(\frac{\pi}{N_{ZC}} (\Delta f T_{SEQ} \pm k))} \right|^2 . \end{aligned} \tag{17}$$

Because the length of the *ZC* sequence is equal to 839 and d_u is equal to 280 for the high-speed mode, the PDP should be divided into three windows with length d_u, as shown in Fig. 2. The negative window, main window and positive window with N_{cs} length are set as $l = -d_u$, $l = 0$ and $l = d_u$, respectively.

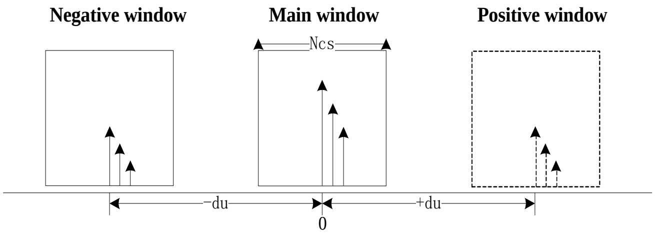

Fig. 2. Power delay profile.

Because the PDP only contains three windows, when the peak power of $P(l)$ at $l = -2d_u$ will coincide with that of $P(l)$ at $l = d_u$ and when the peak power of $P(l)$ at $l = 2d_u$ will coincide with that at $l = -d_u$, we can get

$$P'_{l=0}(\Delta f) = P_{l=0}(\Delta f) \tag{18}$$

$$\begin{aligned} P'_{l=d_u}(\Delta f) &= P_{l=d_u}(\Delta f) + P_{l=-2d_u}(\Delta f) \\ &= \left| \frac{\sin\left(\pi(\Delta f T_{SEQ} + 1) \right)}{\sin\left(\frac{\pi}{N_{ZC}} (\Delta f T_{SEQ} + 1) \right)} \right|^2 + \left| \frac{\sin\left(\pi(\Delta f T_{SEQ} - 2) \right)}{\sin\left(\frac{\pi}{N_{ZC}} (\Delta f T_{SEQ} - 2) \right)} \right|^2 \end{aligned} \tag{19}$$

$$P'_{l=-d_u}(\Delta f) = P_{l=-d_u}(\Delta f) + P_{l=2d_u}(\Delta f)$$
$$= \left| \frac{\sin\left(\pi(\Delta f T_{SEQ} - 1)\right)}{\sin\left(\frac{\pi}{N_{ZC}}(\Delta f T_{SEQ} - 1)\right)} \right|^2 + \left| \frac{\sin\left(\pi(\Delta f T_{SEQ} + 2)\right)}{\sin\left(\frac{\pi}{N_{ZC}}(\Delta f T_{SEQ} + 2)\right)} \right|^2 . \tag{20}$$

Fig. 3 shows the curves of the peak power of the PDP $P'_{l=0}(\Delta f)$, $P'_{l=d_u}(\Delta f)$ and $P'_{l=d_u}(\Delta f)$. From Fig. 3 and the above Eqs. (18)-(20), we can get the following results:

Result: If the frequency offset $\Delta f \in [0\text{Hz}, 1875\text{Hz}]$, then the peak power of $P(l)$ at $l = d_u$ will be bigger than the peak power of $P(l)$ at $l = -d_u$. Meanwhile, when the frequency offset $\Delta f \in [-1875\text{Hz}, 0\text{Hz}]$, the peak power of $P(l)$ at $l = -d_u$ will be bigger than the peak power of $P(l)$ at $l = d_u$. Therefore, according to this principle, we can determine the sign of the frequency offset.

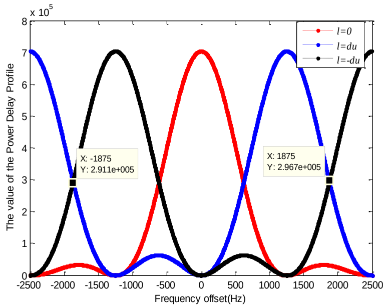

Fig. 3. The curves of the peak power of the PDP with $l = 0$ and $l = \pm d_u$.

As analysed above, the ratio of the peak power of $P'_{l=0}(\Delta f)$, $P'_{l=d_u}(\Delta f)$ and $P'_{l=d_u}(\Delta f)$ can be used to estimate the frequency offset. The range of the FOE of the phase differential algorithm [23, 39] based on PUSH is [−1000 Hz, 1000 Hz], but our proposed scheme based on PRACH can extend the range of FOE to [−1875 Hz, 1875 Hz]. The main steps of the proposed FOE algorithm based on PRACH are as follows:

Step 1: We need to calculate $P(l)$ using Eq. (14).
Step 2: At the main window, positive window and negative window, we need to find the peak power of $P(l)$, which can be denoted as $P'_{l=0}$, $P'_{l=d_u}$ and $P'_{l=d_u}$, respectively.
Step 3: Comparing the value between $P'_{l=d_u}$ and $P'_{l=d_u}$, we can determine the sign of the frequency offset, which is negative or positive. If $P'_{l=d_u} \geq P'_{l=-d_u}$, then the sign of the frequency offset is positive; else, the sign of the frequency offset is negative.
Step 4: Then, we can calculate the PPR value R with the following equation:

$$R = \begin{cases} \dfrac{P'_{l=0}}{\max\left(P'_{l=d_u}, P'_{l=-d_u}\right)} & when\ P'_{l=0} \geq \min\left(P'_{l=d_u}, P'_{l=-d_u}\right) \\ \dfrac{P'_{l=d_u}}{P'_{l=-d_u}} & when\ P'_{l=0} < \min\left(P'_{l=d_u}, P'_{l=-d_u}\right) \end{cases} . \tag{21}$$

Step 5: Lastly, we can derive the value of FOE by referring to the R in the table. The table can be listed by a one-to-one map function between the PPR R and frequency offset Δf. With Eqs. (18)-(21), we can get the following:

When $P'_{l=0} \geq \min(P'_{l=d_u}(\Delta f), P'_{l=-d_u}(\Delta f))$,

$$R(\Delta f) = \frac{P'_{l=0}(\Delta f)}{\max\left(P'_{l=d_u}(\Delta f), P'_{l=-d_u}(\Delta f)\right)}; \tag{22}$$

else,

$$R(\Delta f) = \frac{P'_{l=d_u}(\Delta f)}{P'_{l=-d_u}(\Delta f)}. \tag{23}$$

Through the above description, a novel FOE method based on PRACH, which mainly calculates the PPR of PDP, was proposed. Because the peak power of PDP is greatly affected by noise, the proposed FOE algorithm is less accurate. Because the deviation accuracy of the FOE based on the proposed method is not high, we will introduce a new joint frequency offset method by the conventional frequency estimation [23, 39] based on PUSCH and the proposed FOE based on PRACH.

5. PROPOSED JOINT FOE METHOD

Because the range of the conventional FOE is [–1000 Hz, 1000 Hz], to expand the scope and guarantee the accuracy of the FOE, this paper proposes a joint FOE method, which combines the conventional frequency estimation [23, 39] based on PUSCH and the proposed FOE based on PRACH. The conventional frequency estimation [23, 39] based on PUSCH can be given by

$$\begin{aligned}\Delta f'_{PUSCH} &= \frac{\arg\left(e^{j2\pi N_d T_s \Delta f} \sum_{k=0}^{L-1} H_1(k)^* H_2(k)\right)}{2\pi N_d T_s} \\ &\approx \frac{\arg\left(e^{j2\pi N_d T_s \Delta f}\right)}{2\pi N_d T_s}\end{aligned} \tag{24}$$

where $N_d T_s = 0.5$ms. Δf is the real frequency offset of the transmitting signal $s_i(t)$. If Δf is in the range of [−1000 Hz, 1000 Hz], then we can get $2\pi N_d T_s \Delta f \in [-\pi, \pi]$. Then, Eq. (24) can be expressed as

$$\Delta f'_{PUSCH} \approx \frac{\arg\left(e^{j2\pi N_d T_s \Delta f}\right)}{2\pi N_d T_s} = \frac{2\pi N_d T_s \Delta f}{2\pi N_d T_s} \approx \Delta f. \tag{25}$$

If Δf is in the range of [1000 Hz, 2000 Hz], then $2\pi N_d T_s \Delta f \in (\pi, 2\pi]$, and Eq. (24) can be expressed as

$$\Delta f'_{PUSCH} \approx \frac{\arg\left(e^{j2\pi N_d T_s \Delta f}\right)}{2\pi N_d T_s} \tag{26}$$

$$\approx \Delta f - \frac{1}{N_d T_s}.$$

Thus, the deviation between $\Delta f'_{PUSCH}$ and Δf is $1/N_d T_s$. To correct the error, the estimation frequency offset $\Delta f''$ can be given as

$$\Delta f'' = \frac{1}{N_d T_s} + \Delta f'_{PUSCH} = \Delta f'_{PUSCH} + 2000. \tag{27}$$

Through the above analysis, if Δf is in the range of [−2000 Hz, −1000 Hz], then we can get that

$$\Delta f'' = \Delta f'_{PUSCH} - \frac{1}{N_d T_s} = \Delta f'_{PUSCH} - 2000. \tag{28}$$

Because the range of the proposed PPR method based on PRACH is [−1875 Hz, 1875 Hz], we can use the estimation frequency offset of the proposed PPR based on PRACH to judge the range of the real frequency offset. The joint FOE method is given as below:

Step 1: Use the proposed PPR method to estimate the initial frequency offset $\Delta f'_{PRACH}$ based on PRACH.
Step 2: Use the conventional method to estimate the initial frequency offset $\Delta f'_{PRACH}$ based on PUSCH.
Step 3: Use the estimation frequency offset $\Delta f'_{PRACH}$ to judge the range of the real frequency offset and to correct the estimation frequency offset $\Delta f'_{PRACH}$.

6. SIMULATION RESULTS

In this section, we compare the performance of our proposed algorithms, including the PPR FOE method and joint FOE method, with the conventional cross-correlation FOE algorithm. The simulation model is built based on an LTE system and the AWGN/EPA/EVA/ETU channel models. Tab. 1 shows the system parameters used in the simulation for the conventional cross-correlation FOE algorithm [23, 39] and our proposed algorithms. MATLAB software is used to run this simulation.

Table 1. Simulation parameters for the conventional cross-correlation FOE algorithm and the proposed PPR FOE algorithm.

Parameter	Proposed PPR FOE scheme	Conventional FOE scheme
System bandwidth	20 MHz	20 MHz
Carrier frequency	1 GHz	1GHz
Channel model	AWGN/EPA/EVA/ETU	AWGN/EPA/EVA/ETU
PUSCH RB number	/	50
Preamble format	3	/
PRACH Configuration Index	51	/
Logical root sequence number	384	
Zero correlation zones of length	0	/

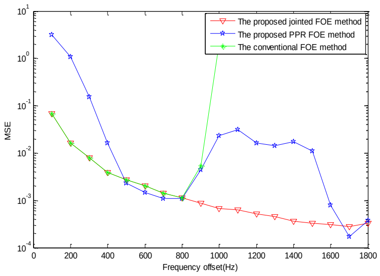

Fig. 4. MSE for the AWGN channel model.

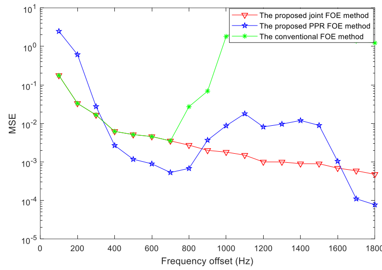

Fig. 5. MSE for the EPA channel model.

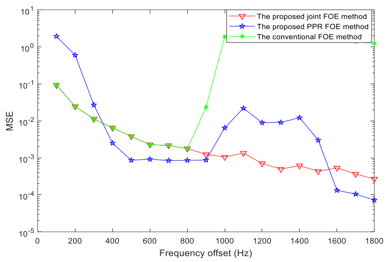

Fig. 6. MSE for the EVA channel model.

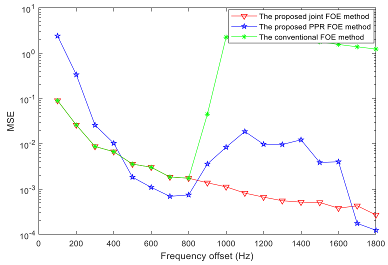

Fig. 7. MSE for the ETU channel model.

Figs. 4-7 compare the normalised mean square error of the conventional algorithms [23, 39] with our proposed algorithms based on the LTE system and the AWGN/EPA/EVA/ETU channel model.

Compared with the conventional FOE and PPR FOE, the proposed joint FOE not only has a wide estimation range but also yields better performance. Our proposed joint FOE widens the estimation range from [−1000 HZ, 1000 Hz] to [−1875 Hz, 1875 Hz] and has the same performance with the conventional FOE based on the LTE system and AWGN/EPA/EVA/ETU channel model.

In this paper, we propose a joint FOE algorithm, which uses a new PPR FOE algorithm based on PRACH and the conventional FOE based on PUSCH in the LTE UL. The joint FDE algorithm combines the advantages of the two algorithms, while taking into account the accuracy and reliability of frequency offset estimation. For the frequency synchronisation of OFDM-based ultra-high-speed environments, such as the satellite communications and the land–air wireless communication system, our proposed joint FOE method can be used to enhance the range of the FOE. The algorithm avoid the problems of high complexity [15] and low estimation accuracy of the previous algorithm [2]. Besides, we also compare the previous algorithm [23, 39] with the algorithm proposed in this article. It's obvious that the joint FOE algorithm is are better than other existing algorithms in different channel model.

Considering the subsequent development of FOE algorithm and the development of AI, we hope to combine the joint FOE algorithm and AI which can help further reduce the complexity of the algorithm. On the one hand, deep learning or reinforcement learning can be used to speed up or improve the accuracy of the algorithm. On the other hand, the proposed joint algorithm results can be used as the input of the training set in the AI to improve the training accuracy.

7. CONCLUSION AND FUTURE WORK

This paper draws on the experience of the conventional FOE algorithms and designs a joint FOE algorithm. From the simulation results in this paper, we know that our joint FOE algorithm can expand the estimation range of frequency offset and improve the accuracy of frequency offset estimation. This result is obvious, because we combine the advantages of multiple FOE algorithms, consider the coupling of the steps in the joint algorithm, and deeply consider the characteristics of frequency offset, so we can obtain a larger range of frequency offset estimation.

Although the joint FOE algorithm we designed has better performance than the traditional FOE algorithm, there is still room for improvement in the time complexity of the joint FOE algorithm, so our future work hopes to reduce the algorithm complexity of the joint FOE algorithm and ensure the estimation accuracy. Under the needs of AI, use AI to improve the efficiency of joint algorithms.

REFERENCES

1. V. D. B. Jan-Jaap, M. Sandell, and P. O. Borjesson, "ML estimation of time and frequency offset in OFDM systems," *IEEE Transactions on Signal Processing*, Vol. 45, 1997, pp. 1800-1805.
2. J. C. Lin, "Maximum-likelihood frame timing instant and frequency offset estimation for OFDM communication over a fast Rayleigh-fading channel," *IEEE Transactions on Vehicular Technology*, Vol. 52, 2003, pp. 1049-1062.
3. N. N. Chen, X. T. Gong, Y. M. Wang, *et al.*, "Random clustering forest for extended belief rule-based system," *Soft Computing*, Vol. 25, 2021, pp. 4609-4619.
4. R. Cheng, W. Yu, Y. Song, *et al.*, "Intelligent safe driving methods based on hybrid automata and ensemble CART Algorithms for multihigh-speed trains," *IEEE Transactions on Cybernetics*, Vol. 49, 2019, pp. 3816-3826.
5. H. Cheng, L. Wu, R. Li, *et al.*, "Data recovery in wireless sensor networks based on attribute correlation and extremely randomized trees," *Journal of Ambient Intelligence and Humanized Computing*, Vol. 12, 2021, pp. 245-259.
6. Y. Cheng, H. Jiang, F. Wang, *et al.*, "Using high-bandwidth networks efficiently for fast graph computation," *IEEE Transactions on Parallel and Distributed Systems*, Vol. 30, 2019, pp. 1170-1183.
7. Y. Dai, S. Wang, X. Chen, *et al.*, "Generative adversarial networks based on Wasserstein distance for knowledge graph embeddings," *Knowledge-Based Systems*, Vol. 190, 2020, pp. 105165.
8. R. Mo, Y. H. Chew, T. Tjhung, *et al.*, "A new blind joint timing and frequency offset estimator for OFDM systems over multipath fading channels," *IEEE Transactions on Vehicular Technology*, Vol. 57, 2008, pp. 2947-2957.
9. Y. G. Fu, H. Y. Huang, Y. Guan, *et al.*, "EBRB cascade classifier for imbalanced data via rule weight updating," *Knowledge-Based Systems*, Vol. 223, 2021, p. 107010.
10. V. D. B. Jan-Jaap, P. O. Borjesson, M. L. Boucheret, *et al.*, "A time and frequency synchronization scheme for multiuser OFDM," *IEEE Journal on Selected Areas in Communications*, Vol. 17, 1999, pp. 1900-1914.

11. Y. G. Fu, J. F. Ye, Z. F. Yin, *et al*., "Construction of EBRB classifier for imbalanced data based on fuzzy C-means clustering," *Knowledge-Based Systems*, Vol. 234, 2021, p. 107590.
12. M. H. Hsieh and C. H. Wei, "A low-complexity frame synchronization and frequency offset compensation scheme for OFDM systems over fading channels," *IEEE Transactions on Vehicular Technology*, Vol. 48, 1999, pp. 1596-1609.
13. Y. G. Fu, J. H. Zhuang, Y. P. Chen, *et al*., "A framework for optimizing extended belief rule base systems with improved ball trees," *Knowledge-Based Systems*, Vol. 210, 2020, p. 106484.
14. N. Lashkarian and S. Kiaei, "Class of cyclic-based estimators for frequency-offset estimation of OFDM systems," *IEEE Transactions on Communications*, Vol. 48, 2001, pp. 2139-2149.
15. S. Ma, X. Pan, G. H. Yang, *et al.*, "Blind symbol synchronization based on cyclic prefix for OFDM systems," *IEEE Transactions on Vehicular Technology*, Vol. 58, 2009, pp. 1746-1751.
16. T. Fusco and M. Tanda, "Blind synchronization for OFDM systems in multipath channels," *IEEE Transactions on Wireless Communications*, Vol. 8, 2009, pp. 1340-1348.
17. L. Guo, M. Li, and D. Xu, "Efficient approximation algorithms for maximum coverage with group budget constraints," *Theoretical Computer Science*, Vol. 788, 2019, pp. 53-65.
18. X. Ma, C. Tepedelenlioğlu, G. B. Giannakis, *et al.*, "Non-data-aided carrier offset estimators for OFDM with null subcarriers: identifiability, algorithms, and performance," *Selected Areas in Communications*, Vol. 19, 2006, pp. 2504-2515.
19. X. Y. Li, W. Lin, X. Liu, *et al.*, "Completely independent spanning trees on BCCC data center networks with an application to fault-tolerant routing," *IEEE Transactions on Parallel and Distributed Systems*, Vol. 33, 2022, pp. 1939-1952.
20. S. Barbarossa, M. Pompili, and G. B. Giannakis, "Channel-independent synchronization of orthogonal frequency division multiple access systems," *IEEE Journal on Selected Areas in Communications*, 2002, Vol. 20, pp. 474-486.
21. G. Liu, X. Chen, R. Zhou, *et al.*, "Social learning discrete particle swarm optimization based two-stage X-routing for IC design under intelligent edge computing architecture," *Applied Soft Computing*, Vol. 10, 2021, p. 107215.
22. H. Liu and U. Tureli, "A high-efficiency carrier estimator for OFDM communications," *IEEE Communications Letters*, Vol. 1, 1997, pp. 104-106.
23. P. H. Moose, "A technique for orthogonal frequency division multiplexing frequency offset correction," *IEEE Transactions Communications*, Vol. 42, 1994, pp. 2908-2914.
24. T. M. Schmidl and D. C. Cox, "Robust frequency and timing synchronization for OFDM," *IEEE Transactions Communications*, Vol. 45, 1997, pp. 1613-1621.
25. U. Mengali and M. Morelli, "Data-aided frequency estimation for burst digital transmission," *IEEE Transactions Communications*, Vol. 45, 1997, pp. 23-25.
26. G. Liu, Z. Chen, Z. Zhuang, *et al.*, A unified algorithm based on HTS and self-adapting PSO for the construction of octagonal and rectilinear SMT," *Soft Computing*, Vol. 24, 2020, pp. 3943-3961.
27. B. Dongming, Z. Gengxin, and Y. Xinying, "A maximum likelihood based carrier frequency estimation algorithm," in *Proceedings of the 5th International Conference on Signal Processing*, 2000, pp. 185-188.

28. Y. Chunlin, L. Shaoqian, T. Youxi, *et al.*, "A novel frequency offset estimation method for OFDM systems with large estimation range," *IEEE Transactions on Broadcasting*, Vol. 42, 2006, pp. 58-61.
29. G. Liu, X. Zhang, W. Guo, *et al.*, "Timing-aware layer assignment for advanced process technologies considering via pillars," *IEEE Transactions on Computer-Aided Design of Integrated Circuits and Systems*, Vol. 41, 2022, pp. 1957-1970.
30. O. Weikert, "Joint estimation of carrier and sampling frequency offset, phase noise, IQ offset and MIMO channel for LTE advanced UL MIMO," in *Proceedings of IEEE 14th Workshop on Signal Processing Advances in Wireless Communications*, 2013, pp. 520-524.
31. T. Koivisto, T. Kuosmanen, and T. Roman, "Estimation of time and frequency offsets in LTE coordinated multi-point transmission," in *Proceedings of IEEE Vehicular Technology Conference*, 2013, pp. 1-5.
32. K. F. Guo, W. Xu, and G. X. Zhou, "Differential carrier frequency offset and sampling FOE for 3GPP LTE," in *Proceedings of IEEE Vehicular Technology Conference*, 2011, pp. 1-5.
33. G. Liu, Y. Zhu, S. Xu, Y. C. Chen, and H. Tang, "PSO-based power-driven X-routing algorithm in semiconductor design for predictive intelligence of IoT applications," *Applied Soft Computing*, Vol. 114, 2022, pp. 108-114.
34. Z. Lu, G. Liu, and S. Wang, "Sparse neighbor constrained co-clustering via category consistency learning," *Knowledge-Based Systems*, Vol. 201, 2020, p. 105987.
35. N. Liu, J. Pan, C. Sun, and S. C. Chu, "An efficient surrogate-assisted quasi-affine transformation evolutionary algorithm for expensive optimization problems," *Knowledge-Based Systems*, Vol. 209, 2020, p. 106418.
36. S. Shen, Y. Yang, and X. Liu, "Toward data privacy preservation with ciphertext update and key rotation for IoT," *Concurrency and Computation: Practice and Experience*, 2021, No. e6729.
37. S. Wang, Z. Wang, K. L. Lim, *et al.*, "Seeded random walk for multi-view semi-supervised classification," *Knowledge-Based Systems*, Vol. 222, 2021, p. 107016.
38. Z. Yu, X. Zheng, F. Huang, W. Guo, L. Sun, and Z. Yu, "A framework based on sparse representation model for time series prediction in smart city," *Frontiers of Computer Science*, Vol. 15, 2021, pp. 1-13.
39. J. Liu, B. Wu, and P. A. Li, "On timing offset and FOE in LTE uplink," *Wireless Communications and Applications*, LNCS, Vol. 72, 2012, pp. 265-274.
40. J. Wang, B. Guan, S. Y. Liu, *et al.*, "Frequency offset estimation based on peak power ratio in LTE system," *Journal of China Universities of Posts and Telecommunications*, Vol. 20, 2013, pp. 49-54.
41. J. Wang, Q. Z. Qin, S. Y. Liu, *et al.*, "Low complexity joint time offset and frequency offset estimations for LTE uplink system," *Journal of China Universities of Posts and Telecommunications*, Vol. 21, 2014, pp. 30-36.
42. A. S. Namitha and S. M. Sameer, "A novel joint method for frequency offset estimation and peak-to-average power ratio reduction in OFDM systems using null subcarriers," *Wireless Personal Communications*, Vol. 83, 2015, pp. 343-359.
43. Standard: 3GPP TS 36.211 v9.1.0. 3GPP Standard for Evolved Universal Terrestrial Radio Access (EUTRA): Physical channels and modulation, 2010.

Qian Du received the BS degree from Qufu Normal University, Qufu, China in 2004 and received the BS and MS degrees in Communication Engineering from Huazhong Normal University, Wuhan, China, in 2004. She is currently an Associate Professor with the School of Information Science and Engineering, Linyi University, Linyi, China. Her research interests include wireless networks algorithm and Internet of Things, *etc.*

Zhao-Feng Wu is currently working toward the master’s degree with the Hunan University of technology. His research interests include orthogonal time-frequency space modulation and machine learning.

Jun Wang received the MS and Ph.D. degrees in Communication Engineering from Huazhong Normal University, Wuhan, China, in 2007, and 2016, respectively. He is currently an Associate Professor with the School of Physics and Electronic Electrical Engineering, XiangNan University, Chenzhou, China. His research interests include communication algorithm, such as channel estimation, equalizer, encoding/decoding, *etc.*

Wen-Wu Xie received the BS, MS, and Ph.D. degrees in Communication Engineering from Huazhong Normal University, Wuhan, China, in 2004, 2007, and 2017, respectively. He is currently an Associate Professor with the School of Information Science and Engineering, Hunan Institute of Science and Technology, Yueyang, China. His research interests include communication algorithm, such as channel estimation, equalizer, encoding/decoding, *etc.*

Ya-Lan Li received the BS degree from Hunan University of Science and Technology, Xiangtan, China in 2004 and received the MS and Ph.D. degrees in Communication Engineering from Huazhong Normal University, Wuhan, China, in 2007, and 2017, respectively. She is currently an Associate Professor with the School of Physics and Electronic Electrical Engineering, XiangNan University, Chenzhou, China. Her research interests include communication algorithm and pattern recognition, *etc.*